Lab on a Chip

PAPER

View Article Online
View Journal | View Issue

Cite this: *Lab Chip*, 2019, **19**, 2456

Cell sorting actuated by a microfluidic inertial vortex†

Robyn H. Pritchard,[a] Alexander A. Zhukov,[a] James N. Fullerton,[bc] Andrew J. Want,[b] Fred Hussain,[a] Mette F. la Cour,[a] Mikhail E. Bashtanov,[a] Richard D. Gold,[a] Anthony Hailes,[a] Edward Banham-Hall[b] and Salman Samson Rogers *[a]

Received 4th February 2019,
Accepted 27th May 2019

DOI: 10.1039/c9lc00120d

rsc.li/loc

The sorting of specific cell populations is an established tool in biological research, with new applications demanding greater cell throughput, sterility and elimination of cross-contamination. Here we report 'vortex-actuated cell sorting' (VACS), a new technique that deflects cells individually, *via* the generation of a transient microfluidic vortex by a thermal vapour bubble: a novel mechanism, which is able to sort cells based on fluorescently-labelled molecular markers. Using *in silico* simulation and experiments on beads, an immortal cell line and human peripheral blood mononuclear cells (PBMCs), we demonstrate high-purity and high-recovery sorting with input rates up to 10^4 cells per s and switching speeds comparable to existing techniques (>40 kHz). A tiny footprint (1 × 0.25 mm) affords miniaturization and the potential to achieve multiplexing: a crucial step in increasing processing rate. Simple construction using biocompatible materials potentially minimizes cost of fabrication and permits single-use sterile cartridges. We believe VACS potentially enables parallel sorting at throughputs relevant to cell therapy, liquid biopsy and phenotypic screening.

Introduction

Cell sorting has found a vast range of applications in biology, permitting the isolation and study of discrete cell populations. The prevailing technology is the combination of the jet-in-air sorter (JIA) with fluorescence cytometry,[1,2] commonly known as fluorescence-activated cell sorting (FACS). State-of-the-art instruments sort millions of cells within an hour, measuring multiple fluorescent markers simultaneously with sensitivity down to tens of fluorophores per cell. However, several clinical and biotechnology research applications, including cell therapy, liquid biopsy and high-throughput phenotypic screening, are poorly served by JIA due to inherent limitations including throughput, automation, reproducibility and sterility.

Cell therapies, for example autologous chimeric antigen receptor (CAR) T-cell therapies, are currently experiencing vast increases in sophistication. These often demand selection of a rare phenotype at >90% purity from an input population ~10^9 cells, to produce efficacious doses of ~10^9–10^{10} cells.[3–5] The output phenotype is typically defined by a small number of surface markers, and may be a rare subpopulation. For instance, regulatory T-cell (Treg) therapies rely on target cells representing <10% of PBMCs.[6,7] Taken together, it is estimated that therapeutic sorting requires a 10–20× processing rate improvement on JIA instruments *i.e.* ~0.5×10^9 cells per h. Furthermore, therapeutic cell sorting must adhere to good manufacturing practice (GMP): key concerns are elimination of contamination, cross-contamination, and aerosolized biohazards.

High-end JIA sorters typically process PBMCs with high purity, high recovery and high viability at 1–2 × 10^4 cells per s. Throughput is limited by cell viability, resulting from shear rate or pressure drop across the nozzle, and decreases of yield, purity and reliability, caused by a reduction of flow focusing and blocking of the nozzle by cell aggregates.[8,9] Notably, these limitations apply to any single-stream sorter, including the many recently-described microfluidic cell sorting technologies.[10–22]

We believe that the practical route to higher-throughput sorting requires multiplexing: simultaneously operating a parallel array of single-stream sorters. The key challenge to enable high-throughput parallel sorters is to make an individual sorter much smaller and simpler than existing designs,

[a] *TTP PLC, Melbourn Science Park, Melbourn, Cambridgeshire SG8 6EE, UK. E-mail: samson.rogers@ttp.com*
[b] *GlaxoSmithKline Clinical Unit Cambridge, Addenbrookes Hospital, Hills Rd, Cambridge CB2 0QQ, UK*
[c] *Applied Biomedical Engineering Group, Division of Medicine, University College London, Rayne Building, 5 University Street, London, WC1E 6JF, UK*
† Electronic supplementary information (ESI) available. See DOI: 10.1039/c9lc00120d

without sacrificing switching speed. For example, $\sim 0.5 \times 10^9$ cells per h would be satisfied by 16 sorters, each processing 10 000/s. However, arranged as a 4 × 4 array on chip, the pitch must be ≤1 mm to achieve sufficient sensitivity with reasonable optical components (lenses and filters ≤2 inch diameter). While several parallel flow cytometers[23–29] and one parallel sorter[30] have been published, until now no microfluidic cell sorters meet this specification, because of their size (including actuators and side-channels), low sort rates, or other complexities.

Here, we present VACS, a unique new sorting mechanism, allowing JIA rates in scalable microfluidic devices, inspired by recent discoveries in inertial microfluidics.[31–36]

Notably, inertial vortices have already been created in microfluidic devices and used for particle separation or enrichment effects.[32–36] What distinguishes VACS from the prior art, is that in VACS, the vortex is transiently created by the interaction of a fast electronic actuator with the channel geometry; the vortex is then shed and flows downstream. These lead to the innovative use of the vortex in cell sorting: *i.e.* VACS selects single particles in the flow, based on optical cytometry. In the prior art, in contrast, vortices are created by the interaction of the steady flow with the channel geometry: these vortices persist at certain positions while particles enter them and migrate to different paths according to how their physical properties are affected by the fluid flow. Thus VACS is able to sort particles based on fluorescently labelled markers, while the prior art separates particles based on size, density or other physical differences.

A thermal inkjet (TIJ)-style actuator is employed to create fluid displacement, but instead of using the vapour bubble to directly displace cells,[15–18] the bubble creates a transient inertial vortex, *i.e.* rotational flow at a well-defined position in the stream. Actuation by TIJ is attractive because the actuator itself, a thin-film microresistor, is small relative to the target pitch (typical dimension ~100 μm (ref. 18)) and can be made using standard micro-electro-mechanical-systems (MEMS) methods, from bio-compatible materials such as titanium and gold on a glass substrate.[37,38] TIJ actuators have been developed and studied extensively over four decades for use in the digital printing industry. The benefit of using rotational flow rather than direct deflection is that smaller bubbles of shorter lifetime can be used, without necessitating side channels to focus the displacement in the deflection region.[15,17] This allows a much smaller and faster sorter device.

We therefore believe that VACS has potential advantages for practical miniaturization and multiplexing of high-throughput cell sorting.

Methods

The vortex-actuated cell sorters were designed and tested by multiphysics simulation, to test the core physical concepts before they were built. The COMSOL models (COMSOL AB, Stockholm, Sweden) are fully described in ESI† 2.1. The devices were then built by standard microfabrication methods, namely thin-film deposition of metals on a glass substrate, followed by casting in PDMS, alignment and bonding of a microfluidic layer (fabrication steps described in ESI† 2.2).

The first experimental evidence of deflection *via* the transient inertial vortex was achieved by setting up a pulsed laser rig, to create thermal vapour bubbles within a channel. The transfer from a laser pulses of defined energy to a bubble was done by adding an absorption dye to the liquid medium. This was a convenient method as it allows a direct control of energy transfer to the thermal vapour bubble and does not require the fabrication of microresistors. Although we did not take this method further, nor test it in an integrated sorter instrument, we describe it in ESI† 2.3 for completeness.

Experiments then progressed to setting-up and evaluating an integrated fluorescence-activated sorter system. VACS chips incorporating an electrical microresistor as the thermal vapour bubble actuator, were mounted in a custom-built fluorescence-activated cytometry rig. ESI† 2.4 describes the cytometry optics, while ESI† 2.5 describes the electronic control system. A syringe pump with a 5 mL disposable syringe was used to introduce particle suspensions at a defined volumetric flow rate into the VACS chip. The two outlets of the VACS chip (sort and waste ports) were piped to 15 mL centrifuge tubes to collect the sort and waste outputs respectively.

Quantitative experimental evaluation of the core device was done first using strobe microscopy which gives a direct means to evaluate sort efficiency by observing individual sort events (strobe set-up described in ESI† 2.6). The strobe LED and camera were triggered by detection of positive events, thus enabling precise measurement of bead position with arbitrary timing, in an uncorrelated sample of sort events. In one configuration, the strobe LED was set up to flash twice with configurable delay times to image the particle in two positions in the same frame: firstly at the maximum extent of the thermal vapour bubble, and secondly after passing the junction into sort and waste channels. In this way, we were able to measure statistics of correctly sorted particles. Various parameters were explored: the actuation delay time (position of particle at time of actuation), feature dimensions of the VACS device (including the channel dimensions, microresistor dimensions and inertial focusser dimensions), flow rates, particle densities, the actuation pulse (voltage, duration), and the control system (minimum repeat time, coincidence detection and abort).

We then evaluated the sorting of populations of microbeads (ESI† 2.7). The purity and recovery of the output was measured, which depends on full system integration: cytometric detection (fluorescence and forward scatter measurement and gating), control system and power electronics (sending appropriately timed pulses of reliable power and duration), the loss of particles by adhesion and sedimentation in vessels and tubing, and the VACS chips (testing production of thermal vapour bubbles, efficiency of deflection over up to millions of particles).

After beads, we progressed to testing the sorter with an immortal cell line (ESI† 2.8) and finally human PBMCs from multiple volunteers (ESI† 2.9). These experiments tested the feasibility of using VACS for viable sorting of living cells.

Human blood was taken from volunteers in accordance with Good Clinical Practice and the Declaration of Helsinki 2013, and local regulations. The protocol was approved by the local ethics committee (07/Q0108/3; National Research Ethics Service, Cambridgeshire 2 Research Ethics Committee) and all study subjects provided written informed consent (n = 7, age range 29–64, 3 female).

The VACS devices use a serpentine inertial focusser as their input: its design and testing is described in ESI† 2.10. The important characteristic of the inertial focusser is lateral position error within the channel that may cause false positive or negative events. We evaluate frequency of outliers in our chosen inertial focusser design.

Two modes of sorting were set up in the control system: high purity and high recovery. In high-purity mode, sort events are aborted if a negative coincidence is detected (*i.e.* detection of a negative particle within the sort envelope). In high-recovery mode, there is no rejection of positive particles, except if they occur within a minimum repeat time parameter. The statistics of the theoretical ideal high-purity and high-recover sorter are described in ESI† 2.11. We compared the experimentally observed sorter performance with these theoretical sorters.

Results

Device concept and simulation

The concept of vortex-actuated cell sorting is as follows: by placing a sharp edge feature in a microchannel of ~100 μm dimension, transient flow caused by a microbubble expansion and collapse may lead to localised inertial rotation in the fluid sufficient to cause particle deflection. Fig. 1(a) shows the device design, which incorporates a TIJ-style microresistor actuator to generate the bubble. Since the velocity due to both the steady flow (prevailing flow through the sorter) and transient flow (caused by the actuator) is significant (both of magnitude around 2 ms^{-1}), the channel Reynolds number is of order 10^2 and therefore both steady and transient flows may cause inertial effects.[39] The Stokes number of a particle such as a 10 μm-diameter cell or polystyrene bead, having a density mismatch of 5–10% with water, is of order 10^{-2}, suggesting that such particles will behave approximately like tracers in the flow: passively tracing the streamlines of steady and transient flows.

Simulation makes a clear prediction of the vortex and its effect on a particle: a vortex is created at the sharp edge feature. If a particle transits the feature coincident with the creation of this vortex, the vortex causes a permanent displacement perpendicular to the streamlines of the steady flow. 2D and 3D simulations of fluid flow in VACS were created in COMSOL (ESI† 2.1, 3.1 and V1–V3). Fig. 1(d) shows a time series: the transient flow creates a vortex at the sharp edge, which is then shed and flows downstream. The vortex deflects a simulated 10 μm polystyrene particle within a narrow region along the flow path. Fig. 1(e) shows trajectories of these simulated particles, showing the direct displacement in the transient flow of only 6 μm, which is fully reversed by collapse of the bubble. However, the subsequent creation of the vortex causes a much larger permanent displacement of around 18 μm by the time the vortex has dissipated approximately 150 μm downstream of the sharp edge.

Note that if we remove mass from the simulation (*i.e.* setting fluid density and particle mass to zero), then the vortex is not created, and no deflection of a particle occurs. Thus the simulation clearly predicts that the particle deflection effect is inertial. This simulation is shown in V4: particles are injected on the centre streamline, and the displacements caused by the actuation are reversible such that no particle deflection occurs.

Also pictured in Fig. 1 is our concept of a 16× parallel microfluidic cell sorter based on this principle (Fig. 1c), laid out on a 4 × 4 array of pitch 1 mm. Although not yet built, it is included to show that the VACS design potentially enables a high density of parallelization on chip. ESI† 2.4 shows a conventional architecture of an optical system for parallel interrogation of these 16 sorters, with an array of laser spots and array detectors for forward scatter, back scatter and fluorescence, each aligned with the image of the sorter array.

Lab-on-chip microfabrication and integration with experimental sorter system

Fig. 1(b) shows the VACS device made by conventional MEMS/lab-on-chip techniques (ESI† 2.2, with variations of the design for experiments described). The microheater is a sputtered layer of titanium on a borosilicate glass substrate, while the conductor tracks are gold on a titanium adhesion layer. The microchannels are cast in a layer of PDMS, bonded to the glass substrate by plasma surface treatment.

The experimental sorter rig integrates optical detection (fluorescence, forward scattering, back scattering, bright-field transmission strobe imaging, as described in ESI† 2.4), a VACS chip with an 80 × 180 μm microheater, an FPGA-based control system to decide which particles to deflect (ESI† 2.5), and an image analysis algorithm to analyse the strobe images and verify a sample of the sorting events (ESI† 2.6). Suspensions of particles are focused by an inertial focusing element and carried at a centre-stream velocity of around 2 ms^{-1} in the sorting region (ESI† 2.10). The particles are analysed optically at the laser focus, approximately 200 μm upstream of the sort envelope. Control logic is set up on the FPGA with a 'firing delay time' between the detection and the microheater pulse; this delay time is scanned to determine the 'sort envelope'.

Applying electrical current to the microresistor causes rapid heating, which nucleates a thermal vapour bubble. The design and development of the actuator is described in ESI† 3.3; the size and lifetime of the bubble has a complicated dependence on the size of the heater, the power dissipation rate, and the dynamic resistance of the channel.

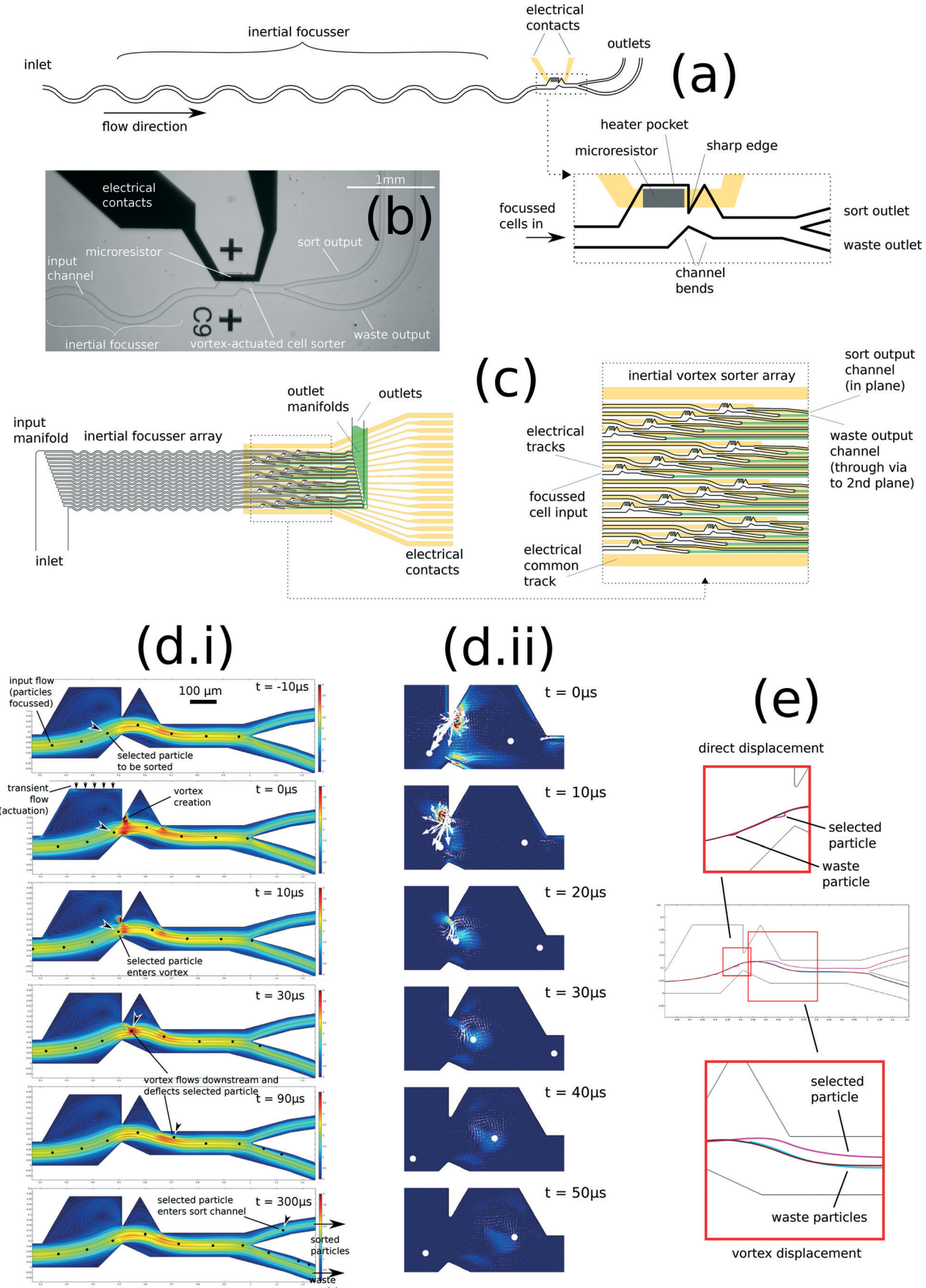

Fig. 1 Concept and simulation of VACS. (a) The VACS design incorporating several extra features: a symmetric serpentine inertial focusser, a heater pocket to put a safe distance between the hot vapour bubble and the particles to be sorted, and a pair of bends in the channel, to direct the particles closer to the vortex-creating edge. (b) Assembled VACS device on a microfluidic sorter chip, made using MEMS and lab-on-chip techniques. (c) Multiplex sorter device, currently in development, enabled by the vortex sorter. (d) 2D fluid flow simulation of the vortex sorter, incorporating a steady flow (carrying the particles from the left at 2 ms^{-1} in the centre-stream), a transient flow from the top wall to simulate the thermal vapour bubble, and tracer particles. Two sequences are shown, with time slices relative to the time of maximum bubble extent: (d.i) showing streamlines and the total flow field from −10 μs to 300 μs, by which time the particle has entered the sort channel, and (d.ii) a detail of the transient component of the flow, showing how the vortex is generated at the sharp edge and shed downstream, subsequently decaying over tens of microseconds. (e) Simulated trajectories of tracer particles are plotted to compare deflection caused directly and *via* the vortex. The direct displacement is up to 6 μm and transiently affects not only the selected particle (magenta trace) but two neighbouring particles of 100 μs separation (cyan/brown traces), while the permanent displacement caused by the vortex is 18 μm and only affects the selected particle. The vortex decays within around 150 μm as it flows downstream.

Evaluation of core device and sorter system with microbeads

The sorter was first evaluated with suspensions of 6 μm and 10 μm polystyrene beads, introduced by a syringe pump (experimental conditions described in ESI† 2.7). Strobe microscopy provides a means to sample individual sort events and evaluate the statistics of deflection (described in ESI† 3.4–3.5). A minimum resistor size of 80 × 120 μm was required to sort particles, but reliable high-efficiency sorting required a resistor size of 80 × 180 μm.

Fig. 2(a) and Videos V6 and V7 show examples of strobe microscopy to track particles through the vortex actuation and evaluate individual sort events. The 'sort envelope' represents the ability to pick individual particles from a stream, which is the key performance attribute of the core device. This envelope can be defined spatially (particle position at the time of actuation, along the contour of particle positions), or temporally (delay time of actuation after optical detection of the particle). Ideally, the probability of deflection is 100% within and 0% outside the sort envelope.

Fig. 2(b) shows statistics of 2100 individual events, in which a 10 μm bead was either found to be deflected into the sort channel or undeflected into the waste channel. The histogram of proportion sorted reveals a sort envelope of 52 μm (spatial units) or 23 μs (temporal units), which is the distance or time respectively to go from 0% probability of sorting, to 100% to 0% again. This histogram allows direct estimation of error rates for the device: false positive rate <0.06% and false negative rate <0.25% (ESI† 3.4).

With channel dimensions suitable for PBMCs, our measured sort envelope of 23 μs compares with the 8 μs predicted by simulation: the difference is probably caused by mechanical compliance of the channel walls. We can define a 'sort envelope rate' of 1/(23 μs) = 43 kHz which represents the maximum rate to address individual particles. This may be directly compared with the droplet rate on a JIA sorter, with the caveat that there may be other important rates limiting the thermal vapour bubble generation, as further discussed below. In the case of sorting a rare positive cell subset out of a largely negative population, the sort envelope rate is equivalent to a droplet rate. The demonstration of bead and cell sorting (below) gave purities and recoveries consistent with this sort envelope.

Strobe microscopy also reveals bead deflection by the inertial vortex, shown in Fig. 2(c). These trajectories agree qualitatively with the simulation, in that no permanent deflection occurs in the region of the bubble, but deflection starts from near the sharp edge and gradually increases to a maximum within ~200 μm from the sharp edge. The direct displacement in the firing zone is ~3 μm, while the displacement before the sort junction is ~20 μm. The inertial vortex thus causes a displacement amplification of around 7, in order-of-magnitude agreement with the simulations.

Two other important rates in our system are 'peak sort rate', the inverse of the minimum repeat time of actuation, and 'sustained sort rate', the average rate that we can continuously operate our actuator. We studied peak sort rates in two ways and found that deflection efficiency did not deteriorate noticeably up to a peak sort rate of at least 10 kHz. Firstly, deflection efficiency was measured directly: we found near-100% efficiency at peak sort rates up to 5 kHz (minimum repeat time 200 μs, ESI† 3.5), beyond which it became difficult to use strobe microscopy to count deflected particles unambiguously. Secondly, measuring deflection efficiency indirectly by comparing recovery statistics to a theoretical sorter (see results below), reveals no significant deterioration of recovery at peak sort rates of 10 kHz.

Sustained sort rates in the experimental system were lower than peak sort rates: we found that the microresistors tended to fail faster if we allowed sustained actuation at greater rates. In the sorting experiments presented below, we limited sustained sustained sort rate to 1–2 kHz, which resulted in a typical lifetime of around 2–3 million sort events. By this number of actuation cycles, the microresistor tended to have failed by thermal, mechanical or electrochemical damage. Higher sustained actuation rates tended to reduce the lifetime measured as number of sort events, presumably due to higher stress or temperatures in the microresistor. We note that our current experimental devices lack the passivation and anti-cavitation layers of the analogous TIJ devices that ensure much longer lifetime and much higher sustained actuation rates in otherwise similar conditions, as discussed below.

The overall sorting performance was tested by mixtures of fluorescent and non-fluorescent beads. We sorted firstly 10 μm beads in 'high-recovery' mode (without rejecting coincidence events), and secondly 6 μm beads in 'high-purity' mode (with rejection of coincidence events). Representative results are shown in Fig. 2(d) and Table 1. The output purity and recovery were measured subsequently with a Sysmex

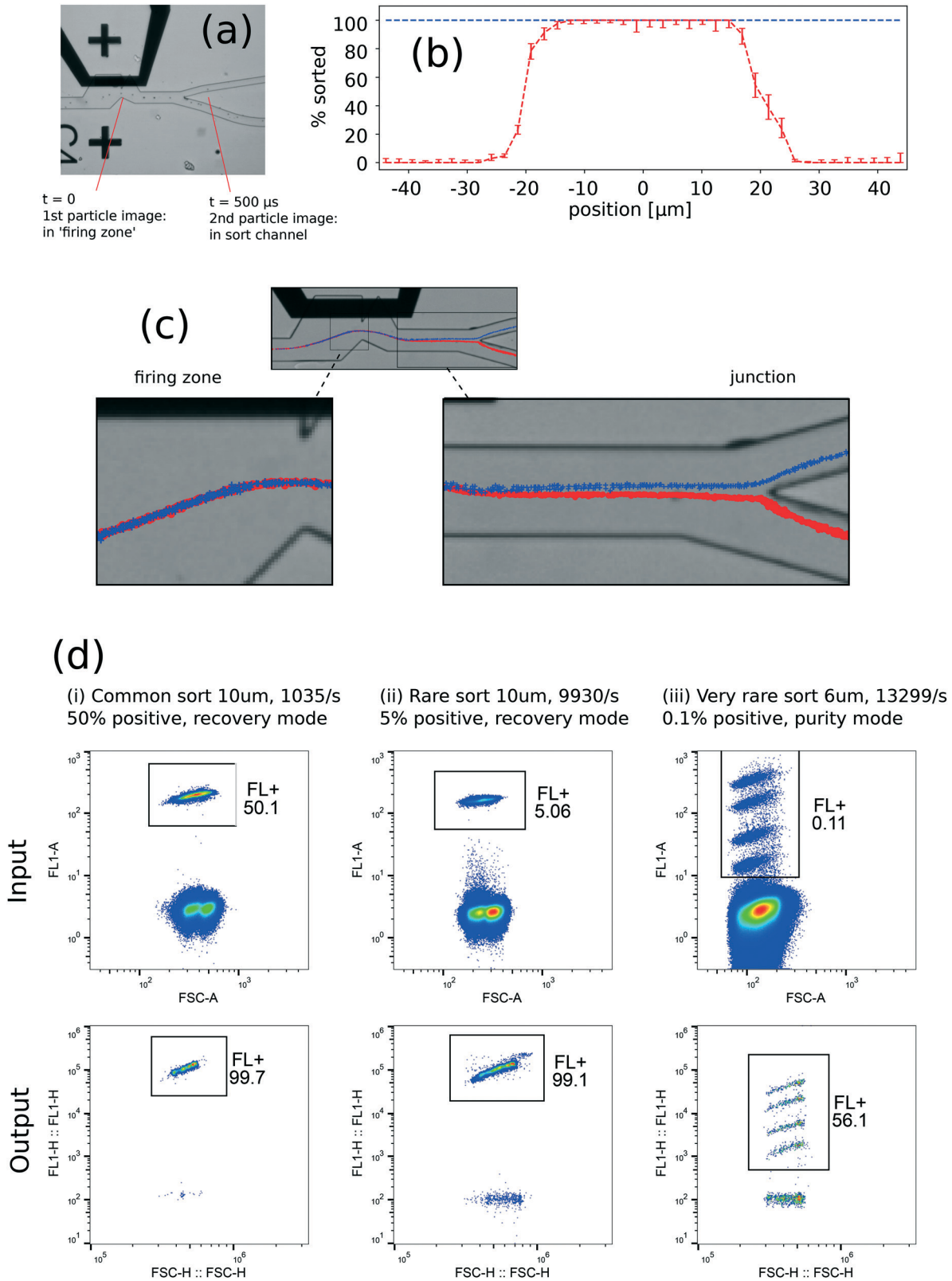

Fig. 2 Demonstration of core device and complete sorter system using polystyrene beads. (a) Double strobe image of a single bead deflected by an inertial vortex out of a stream of 10 μm beads. (b) Sort envelope histogram, containing statistics of 2100 particles. (c) Trajectories of beads going to sort (blue +) and waste (red ○), showing the displacement due to the inertial vortex effect of around 20 μm. (d) Sorting mixtures of fluorescent and non-fluorescent beads. Three mixtures were tested: (d.i) 10 μm beads, common positive, high-recovery mode, 1035/s: pre-sort 50.1% is purified to 99.7% with recovery of 93.5%; (d.ii) 10 μm beads, rare positive, high-recovery mode, 9930/s: pre-sort 5.06% is purified to 99.1% with recovery of 96.9%; and (d.iii) 6 μm beads, very rare positive, high-purity mode, 13 299/s (the top four peaks of the Spherotech RCP-60-5 rainbow beads are sorted from the lower peaks and non-fluorescent beads): pre-sort 0.11% is purified to 56% with recovery of 72%.

Table 1 Sorting results for mixtures of fluorescent and non-fluorescent beads. Purity is defined as the ratio of positive particles to all particles in the sort output. Recovery is defined as the ratio of positive particles in the sort output to positive particles in the input. Theoretical sorter purity and recovery were calculated using the equations in ESI 2.11, taking sort envelope time 23 μs, minimum repeat time of 100 μs and the relevant input rate and pre-sort fraction

Experiment	Bead diameter [μm]	Input rate [/s]	Pre-sort FL+ fraction	Purity	Recovery	Theoretical sorter purity	Theoretical sorter recovery
Common sort, recovery mode	10 μm	1.04×10^3	50.1%	99.7%	93.5%	98.7%	96.7%
Rare sort, recovery mode	10 μm	9.93×10^3	5.06%	99.1%	96.9%	82.3%	96.6%
Very rare sort, purity mode	6 μm	13.3×10^3	0.11%	56.1%	72.1%	100%	73.6%
Deflect all particles, recovery mode	10 μm	1.48×10^3	100%	99.9%	97.5%	100%	90.0%

Partec Cyflow Cube 8 cytometer (Sysmex Partex GmbH, Görlitz, Germany; details in ESI† 2.7).

Sorting results are compared with an ideal 'theoretical sorter', whose only errors are due to coincidence events within the sort envelope (accepting or rejecting coincidences) and minimum repeat time (dropping events), assuming non-correlation of events in the stream. The theoretical sorter's purity and recovery for high-purity and high-recovery modes can be calculated with Poisson statistics (equations given in ESI† 2.11).

In high-recovery mode, both purity and recovery are remarkably close to or higher than the theoretical sorter for our example 'common positive' and 'rare positive' sorts, for input rate 1.04×10^3, positive fraction 50.1%, and 9.93×10^3/s, positive fraction 5.1% respectively. That the integrated instrument achieved purity higher than the theoretical sorter in both cases is likely due to solid sphere exclusion and particle entrainment inertial effects, which cause the arrival of the cells to deviate from Poisson statistics.[31,39] This could be of benefit for high-purity/high-recovery sorting, since coincidence events might be significantly reduced with careful tuning of the design.

In an example 'very rare positive' sort, we processed input rate 1.3×10^4/s and positive fraction 0.11%. We obtained close to the theoretical recovery, but a sort purity of 56%. This would correspond to an error rate of 0.07% false positives.

The final example is a 'deflect all particles' sort, where we processed an input rate of 1500/s and attempted to deflect everything, except events that fell within the 100 μs minimum repeat time. That the recovery is higher than the theoretical sorter recovery in this case is likely due to the non-Poisson arrival time of the events mentioned above. However, it also suggests consistency with the peak sort rate of 10 kHz = 1/(minimum repeat time of 100 μs). The predicted recovery for a peak sort rate of 5 kHz would be approximately 10% lower. That we did not see a loss of performance suggests that deflection efficiency has not dropped greatly at a peak sort rate of 10 kHz.

Evaluation of sorter system with live cells

Second, the sorter was tested with Jurkat cells, an immortal human T-cell line. These were stained to produce an arbitrary fluorescent sub-population and sorted with high recovery (example result in ESI† 3.6). No evidence of cell damage or disruption was evident in light microscopy. Sorted cells continued to proliferate when put back into cell culture media and incubated.

Third, the sorter was evaluated with human PBMCs (ESI† 2.9, 3.7), extracted from heparinised venous blood, taken from healthy volunteers (n = 7).

For proof-of-principle, T-cells (CD3+) and B-cells (CD19+) were sorted, since each can be labelled with a single fluorescent antibody. As arbitrary common and rare compartments respectively, these demonstrate how the sorter could be used for selecting phenotypes in cell therapy. Each labelled sample was resuspended at density 1–2 × 10^6/mL, 5 mL total volume, and sorted in high-purity mode.

Output was measured using standard instruments (a Becton Dickinson FACSCanto II flow cytometer was employed for measuring purity and a Beckman Coulter Z2 Coulter Counter was employed for absolute counting): Fig. 3(a) shows example cytometry gating. Video V8 shows strobe microscopy of PBMC sorting. Fig. 3(b and c) shows full purity and recovery statistics compared with the theoretical sorter. These results are also tabulated fully in Tables S5 and S6† for CD3+ cells, purity averaged 98% (from 63% pre-sort, n = 5). For CD19+ cells, purity averaged 82% (from 1% pre-sort, n = 7). Recovery is close to the expected recovery, allowing for the coincidence rejection and minimum repeat time settings. The difference between sorting performance for beads and PBMCs is likely to be due to defocused cells, ambiguities of gating and coincidence detection, adhesion of cells and counting with external instrumentation.

We expect that refinements of the cytometry optics, control logic, inertial focusser and microchannel material will close this gap. PBMC viability was unaffected by sorting (mean 99.0% pre-sort; 99.5% sort output, n = 4, ESI† 3.8). The devices were observed to be resistant to clogging: we regularly processed ~10^7 PBMCs in each run without failures due to cell aggregation or debris build-up.

Discussion

The VACS concept and its performance have thus been explored on several levels: fluid simulations, strobe microscopy event observations, and finally realistic performance of an integrated fluorescence-activated sorter. The latter has been

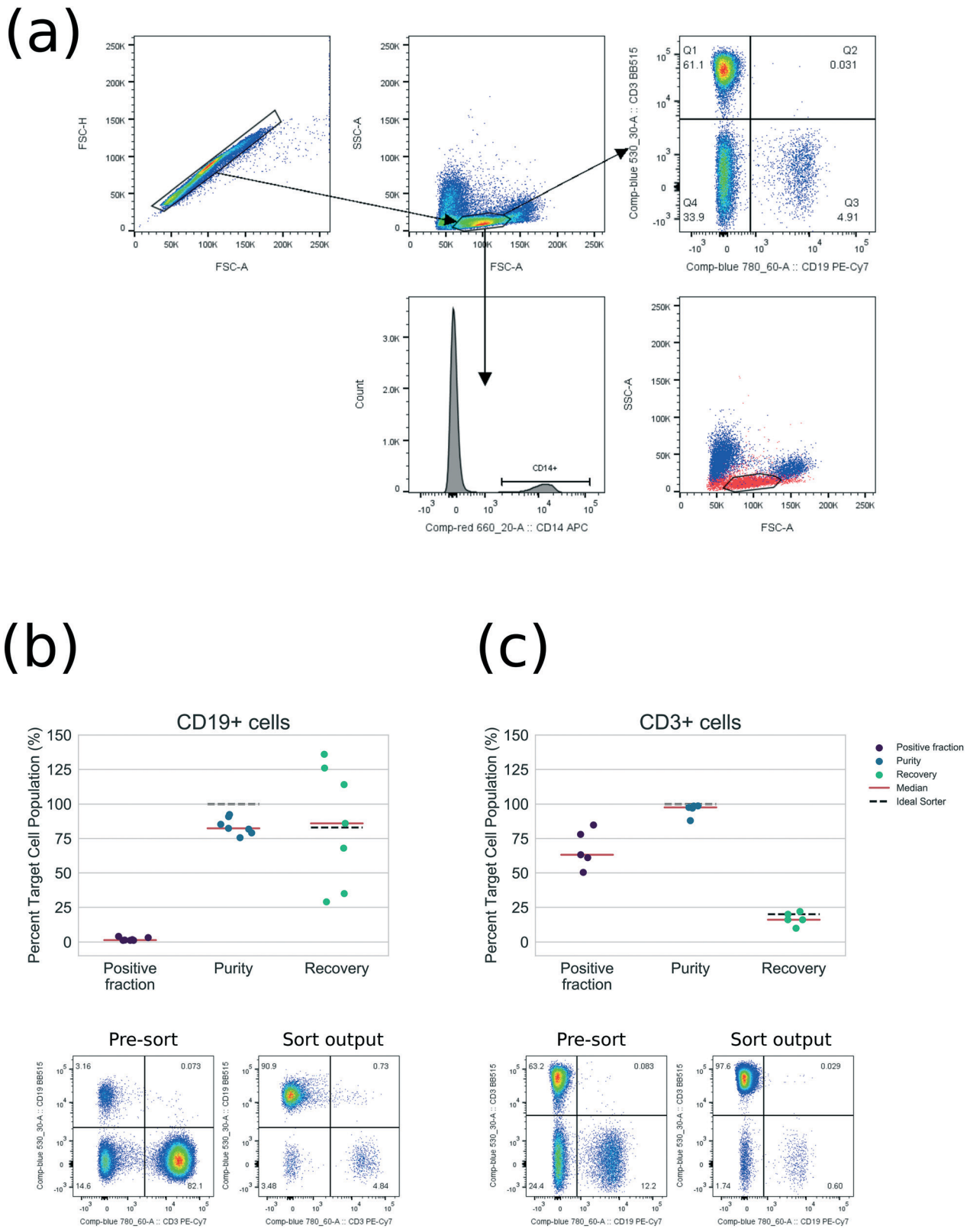

Fig. 3 Evaluation of the sort purity and recovery using human PBMCs. (a) Gating procedure for generation of data from pre- and post-sort CD19/CD3 positive cells. This includes an overlay, backgated from the CD14-positive (monocyte) population, to determine the position of the lymphocyte gate on forward/side scatter plots. Example gating is for pre-sort and sort output data on the standard cytometer. (b and c) Scatter plots showing all data from CD19 and CD3-positive cells respectively (pre-sort positive fraction, sort output purity and recovery), with median values (red line) and median prediction of purity and recovery for an ideal theoretical sorter in high-purity mode (*i.e.* errors due to event coincidences only, taking sort envelope width of 23 μs and minimum repeat time of 100 μs and 1000 μs respectively) (black dashed line). Flow cytometry dot plots are shown below of a representative subject sample from which the scatter plot was derived.

demonstrated with beads, an immortal cell line and human PBMCs from several volunteers.

The main quantitative result is a sort envelope of 23 μs in a device of lateral dimension 250 μm without side channels, which compares favourably to previous microfluidic sorters that employed TIJ-style actuators,[15–18] and is due to the innovation that we have introduced: the generation of a transient inertial vortex. We also included a 16× parallel design (4 × 4 sorters on a 1 mm pitch) to show that the device could potentially be parallelized at a high density on chip.

The current devices are limited by sustained actuation rate (approx. 1 kHz) and lifetime of the microresistor (approx. 2–3 million cycles). In fact, much effort in the early development of TIJ printing was dedicated to successfully solving this problem, by using thin film passivation and anti-cavitation layers to prevent similar failure modes in electrolyte solutions. Commercial devices since over 20 years ago typically achieve sustained actuation rates >15 kHz and lifetimes of billions of cycles.[40] We believe similar microfabrication materials and processes should significantly raise the sustained actuation rates and extend the lifetime of our devices.

Output purity from the current devices seems to be limited by errors in particle focusing. However, for particles of the size of lymphocytes or larger, this only seems to affect purity significantly when approaching positive fraction of the order of 0.1%. This could be reduced by improvements in the inertial focusser design.

In summary, we have invented a novel means of cell sorting, and provided experimental evidence of its functionality. We believe VACS is potentially a disruptive, scalable technology that could enable practical processing of hundreds of millions, to billions of cells in a batch, by high density on-chip multiplexing. A multiplex demonstration rig is in development at the time of writing.

Moreover, the comparative simplicity of the sort mechanism and device construction using biocompatible materials should make VACS suitable for low-cost disposable sorting cartridges. These advantages should enable a variety of research and clinical applications, including cell therapeutic applications, that are currently constrained by existing methods.

Author contributions

RHP, AAZ, MEB, RDG, FH, MLC, SSR: co-inventors of VACS. AAZ, RDG, TH: instrumentation, electronics, firmware and optics. JNF, AJW, EBH: experiments with PBMCs. SSR, RHP, JNF, AJW: data analysis. FH, MLC, RHP: microfabrication. SSR, JF, AJW, RHP, EBH, AAZ: preparing the manuscript.

Data availability statement

The datasets generated and analysed during the current study are available from the corresponding author on reasonable request.

Conflicts of interest

SSR, RHP, AAZ, MEB, RDG, FH, MLC, TH are employees of TTP PLC which is investing in commercial exploitation of the technology. To balance this interest, all experiments on human PBMCs including data collection and analysis were conducted by co-authors JNF, AJW, EBH who have no commercial interest in the technology.

Acknowledgements

The development of VACS was led and funded by TTP PLC, while the GSK Clinical Unit Cambridge contributed the Good Laboratory Practice expertise and facilities to conduct experiments on human blood. JNF is a National Institutes for Health Research (NIHR) Clinical Lecturer seconded to GSK *via* a Medical Research Council (MRC) Proximity to Discovery Award. We thank our many colleagues for advice and input, including Matthew Carr, Giles Sanders, Joanna Maison, Bill Davis, Calum Hayes, Nuno Varelas, Laura Brown, Somer Bexon, Mick Withers, Matthias Edigar, Vidhya Sridhar, Edwin Stone, Hiro Eto, Neil Griffin, Nick Wooder, Wayne Bowen, Alon Greenenko, Richard Janse van Rensburg, Steve Grimwade, Steve Wakefield, Thomas Brown, James Stein, Michael Walker, Paul Galluzzo, Duncan McBryde, Hans Hoppe, Keiko Yata, Allan Sinclair, Drew Glassock, Simon Fisher, Paul Crossman, Steve Taylor, Gary Jepps, Matt Williams.

References

1 M. J. Fulwyler, *Science*, 1965, **150**, 910–911.
2 W. Dittrich and W. Goehde, Flow-Through Chamber for Photometers to Measure and Count Particles in a Dispersion Medium, DE1815352, 1971.
3 J. Corrigan-Curay, H.-P. Kiem, D. Baltimore, M. O'Reilly, R. J. Brentjens, L. Cooper, S. Forman, S. Gottschalk, P. Greenberg, R. Junghans, H. Heslop, M. Jensen, C. Mackall, C. June, O. Press, D. Powell, A. Ribas, S. Rosenberg, M. Sadelain, B. Till, A. P. Patterson, R. C. Jambou, E. Rosenthal, L. Gargiulo, M. Montgomery and D. B. Kohn, *Mol. Ther.*, 2014, **22**, 1564–1574.
4 A. D. Fesnak, C. H. June and B. L. Levine, *Nat. Rev. Cancer*, 2016, **16**, 566–581.
5 M. L. Davila, D. C. G. Bouhassira, J. H. Park, K. J. Curran, E. L. Smith, H. J. Pegram and R. Brentjens, *Int. J. Hematol.*, 2014, **99**, 361–371.
6 N. Safinia, C. Scotta, T. Vaikunthanathan, R. I. Lechler and G. Lombardi, *Immunol. Toler.*, 2015, 438.
7 J. B. Canavan, C. Scottà, A. Vossenkämper, R. Goldberg, M. J. Elder, I. Shoval, E. Marks, E. Stolarczyk, J. W. Lo, N. Powell, H. Fazekasova, P. M. Irving, J. D. Sanderson, J. K. Howard, S. Yagel, B. Afzali, T. T. MacDonald, M. P. Hernandez-Fuentes, N. Y. Shpigel, G. Lombardi and G. M. Lord, *Gut*, 2016, **65**, 584–594.
8 L. W. Arnold and J. Lannigan, in *Current Protocols in Cytometry*, John Wiley & Sons, Inc., 2001.

9 G. Durack and J. P. Robinson, *Emerging Tools for Single-Cell Analysis: Advances in Optical Measurement Technologies*, John Wiley & Sons, 2004.
10 L. Schmid, D. A. Weitz and T. Franke, *Lab Chip*, 2014, **14**, 3710–3718.
11 Z. Ma, Y. Zhou, D. J. Collins and Y. Ai, *Lab Chip*, 2017, **17**, 3176–3185.
12 L. Ren, Y. Chen, P. Li, Z. Mao, P.-H. Huang, J. Rufo, F. Guo, L. Wang, J. P. McCoy, S. J. Levine and T. J. Huang, *Lab Chip*, 2015, **15**, 3870–3879.
13 S. H. Cho, C. H. Chen, F. S. Tsai, J. M. Godin and Y.-H. Lo, *Lab Chip*, 2010, **10**, 1567–1573.
14 C. Lee, J. Lee, H. H. Kim, S.-Y. Teh, A. Lee, I.-Y. Chung, J. Y. Park and K. K. Shung, *Lab Chip*, 2012, **12**, 2736–2742.
15 T.-H. Wu, Y. Chen, S.-Y. Park, J. Hong, T. Teslaa, J. F. Zhong, D. Di Carlo, M. A. Teitell and P.-Y. Chiou, *Lab Chip*, 2012, **12**, 1378.
16 H. Hoefemann, S. Wadle, N. Bakhtina, V. Kondrashov, N. Wangler and R. Zengerle, *Sens. Actuators, B*, 2012, **168**, 442–445.
17 K. de Wijs, C. Liu, A. Dusa, D. Vercruysse, B. Majeed, D. S. Tezcan, K. Blaszkiewicz, J. Loo and L. Lagae, *Lab Chip*, 2017, **17**, 1287–1296.
18 C. C. Chen, J. S. Wang and O. Solgaard, *Sens. Actuators, B*, 2006, **117**, 523–529.
19 *Flow sorters: microchip-based cell sorting technology - Miltenyi Biotec*, http://www.miltenyibiotec.com/en/products-and-services/macs-flow-cytometry/flow-sorter.aspx, (accessed November 14, 2017).
20 Z. Wang, O. Hansen, P. K. Petersen, A. Rogeberg, J. P. Kutter, D. D. Bang and A. Wolff, *Electrophoresis*, 2006, **27**, 5081–5092.
21 L. Wang, L. A. Flanagan, N. L. Jeon, E. Monuki and A. P. Lee, *Lab Chip*, 2007, **7**, 1114–1120.
22 U. Kim, C.-W. Shu, K. Y. Dane, P. S. Daugherty, J. Y. J. Wang and H. T. Soh, *Proc. Natl. Acad. Sci. U. S. A.*, 2007, **104**, 20708–20712.
23 B. W. Buckley, N. Akbari, E. D. Diebold, J. Adam and B. Jalali, *Appl. Phys. Lett.*, 2015, **106**, 123701.
24 D. DiCarlo, A. Ozcan, B. Jalali, S. Hur and H. T. K. Tse, Inertial particle focusing flow cytometer, US8693762 B2, 2014.
25 J. C. K. Chan, E. D. Diebold, B. W. Buckley, S. Mao, N. Akbari and B. Jalali, *Biomed. Opt. Express*, 2014, **5**, 4428–4436.
26 Y. J. Fan, Y. C. Wu, Y. Chen, Y. C. Kung, T. H. Wu, K. W. Huang, H. J. Sheen and P. Y. Chiou, *Biomicrofluidics*, 2013, **7**, 044121.
27 S. C. Hur, H. T. K. Tse and D. D. Carlo, *Lab Chip*, 2010, **10**, 274–280.
28 B. K. McKenna, J. G. Evans, M. C. Cheung and D. J. Ehrlich, *Nat. Methods*, 2011, **8**, 401–403.
29 M. E. Piyasena, P. P. A. Suthanthiraraj, R. W. Applegate, A. M. Goumas, T. A. Woods, G. P. López and S. W. Graves, *Anal. Chem.*, 2012, **84**, 1831–1839.
30 R. Hulspas, L. Villa-Komaroff, E. Koksal, K. Etienne, P. Rogers, M. Tuttle, O. Korsgren, J. C. Sharpe and D. Berglund, *Cytotherapy*, 2014, **16**, 1384–1389.
31 D. Di Carlo, D. Irimia, R. G. Tompkins and M. Toner, *Proc. Natl. Acad. Sci. U. S. A.*, 2007, **104**, 18892–18897.
32 S. C. Hur, A. J. Mach and D. Di Carlo, *Biomicrofluidics*, 2011, **5**, 022206.
33 A. J. Mach, J. H. Kim, A. Arshi, S. C. Hur and D. D. Carlo, *Lab Chip*, 2011, **11**, 2827–2834.
34 X. Wang, J. Zhou and I. Papautsky, *Biomicrofluidics*, 2013, **7**, 044119.
35 X. Wang, X. Yang and I. Papautsky, *Technology*, 2016, **04**, 88–97.
36 H. Haddadi, H. Naghsh-Nilchi and D. Di Carlo, *Biomicrofluidics*, 2018, **12**, 014112.
37 Y. Hong, N. Ashgriz and J. Andrews, *J. Heat Transfer*, 2004, **126**, 259–271.
38 Z. Zhao, S. Glod and D. Poulikakos, *Int. J. Heat Mass Transfer*, 2000, **43**, 281–296.
39 D. D. Carlo, *Lab Chip*, 2009, **9**, 3038–3046.
40 R. Beeson, in *Recent Progress in Ink Jet Technologies II*, Society for Imaging Science and Technology, Springfield, VA, 1998, pp. 27–30.